Published in "The Journal of Physical Chemistry C 120(40): 23286–23292, 2016"
which should be cited to refer to this work.

The Role of Excitons and Free Charges in the Excited-State Dynamics of Solution-Processed Few-Layer MoS_2 Nanoflakes

Demetra Tsokkou,*,† Xiaoyun Yu,‡ Kevin Sivula,‡ and Natalie Banerji*,†

†Department of Chemistry, University of Fribourg, Chemin du Musée 9, CH-1700 Fribourg, Switzerland

‡Laboratory for Molecular Engineering of Optoelectronic Nanomaterials, Institute of Chemical Sciences and Engineering, École Polytechnique Fédérale de Lausanne (EPFL), Station 6, 1015 Lausanne, Switzerland

Supporting Information

ABSTRACT: Solution-processed semiconducting transition metal dichalcogenides are emerging as promising two-dimensional materials for photovoltaic and optoelectronic applications. Here, we have used transient absorption spectroscopy to provide unambiguous evidence and distinct signatures of photogenerated excitons and charges in solution-processed few-layer MoS_2 nanoflakes (10−20 layers). We find that photoexcitation above the direct energy gap results in the ultrafast generation of a mixture of free charges in direct band states and of excitons. While the excitons are rapidly trapped, the free charges are long-lived with nanosecond recombination times. The different signatures observed for these species enable the experimental extraction of the exciton binding energy, which we find to be ∼80 meV in the nanoflakes, in agreement with reported values in the bulk material. Carrier-density-dependent measurements bring new insights about the many-body interactions between free charges resulting in band gap renormalization effects in the few-layer MoS_2 nanoflakes.

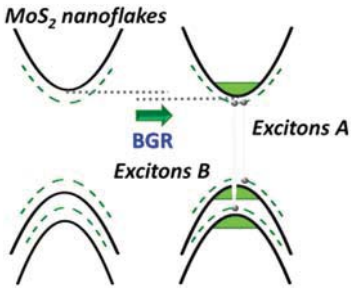

INTRODUCTION

The strong intralayer and weak interlayer interactions in two-dimensional (2D) layered transition metal dichalcogenides give rise to a plethora of novel optical and electrical properties that have recently led to an abundance of research interest in the field.[1−3] Among them, 2H-phase molybdenum disulfide (MoS_2) is an indirect band gap semiconductor, an excellent absorber with excitonic transitions evident at room temperature, and shows a layer-dependent energy band gap.[4−6] Following the progress in processing layers with atomic-size thickness, 2D MoS_2 systems have emerged as strong candidates for next-generation electronics, optoelectronics, and catalysis.[7−11] Initial research concentrated on MoS_2 monolayers,[12−18] where a crossover between the indirect and direct energy band gap leads to enhancement of the photoluminescence quantum yield[5,19] and where strong correlation between excitons and/or charges due to spatial confinement gives rise to the formation of bound trions and biexcitons.[20−22] Later on, it was found that the carrier transport in few-layer nanoflakes improves with the number of layers up to a maximum at about 10 nm thickness (field effect mobility of 700 $cm^2\ V^{-1}\ s^{-1}$ compared to 200 $cm^2\ V^{-1}\ s^{-1}$ in the monolayer)[23] due to the absence of substrate screening in thicker nanoflakes.[24]

The necessity to clarify the fundamental properties of MoS_2 nanoflakes and to unravel the relaxation and/or recombination processes following photoexcitation has motivated extensive studies via ultrafast spectroscopy. The excited-state dynamics in few-layer MoS_2 nanoflakes varies significantly in different studies and depends strongly on the processing route of the samples, showing that additional research is needed to understand their rich photophysics.[12,25−32] Previous transient studies have resolved exciton and charge dynamics, but a clear signature of free charges in the direct conduction and valence bands, which distinguishes them from excitons, has not been previously observed. In addition, time-resolved THz spectroscopy measurements support the presence of free charges in few-layer nanoflakes; however, there are contradictory assignments about the involved energy bands.[17,28,31,32] Differences in the carrier dynamics are expected to arise from different thicknesses of the studied nanoflakes. Also, trapping processes play a significant role in the relaxation/recombination of the carriers due to the atomic thickness of the flakes. Wang et al. have shown increased recombination times with the number of atomic layers due to the interplay between fast picosecond surface recombination and slow nanosecond bulk recombination.[29] Thus, different synthetic methods may have had a significant impact on the distribution and density of trap states and thus on the carrier and exciton dynamics observed previously.[12,25−32] Free carrier dynamics are especially important in view of solar energy conversion, which has been recently encouraged by the development of methods to prepare large area films of solution-processed semiconducting transition metal dichalcogenides.[8,11]

In this work, we report the temporal evolution of photoexcited species in solution-processed MoS_2 nanoflakes with an average thickness of ∼10 nm (∼10−20 atomic layers) using transient absorption (TA) spectroscopy. They were prepared by sonochemically exfoliating bulk MoS_2, and the

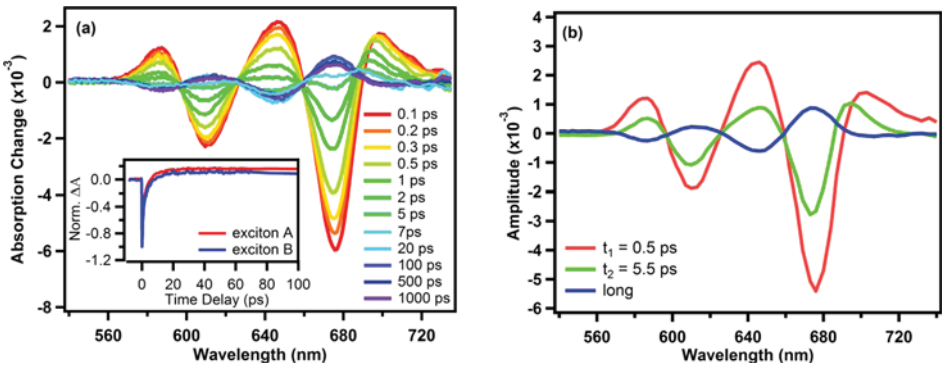

Figure 1. (a) TA spectra in few-layer MoS_2 nanoflakes recorded following photoexcitation at 600 nm at an absorbed pump fluence of ~1.1 μJ/cm^2. In the inset, the temporal evolution of the A and B excitonic resonances is shown. (b) Amplitude spectra for the different relaxation time constants as derived from the multiexponential global analysis of the TA data.

resulting flakes (ca. 100 nm−1 μm in lateral dimension) were processed into thin films via a self-assembly method.[11] It has to be noted that the thickness of these nanoflakes is larger compared to the ones used in previous TA studies (<8 atomic layers).[12,25−27,30,31] We demonstrate that the solution-processed MoS_2 nanoflakes maintain the fundamental properties shown by similar materials prepared using other synthetic methods and thus remain suitable for solar energy conversion. Moreover, we present clear evidence for the ultrafast photogeneration of a mixture of excitons and free charges for excitation above the direct band gap. For the first time, we distinguish between the energy levels of the excitons and the direct conduction/valence band levels and estimate the A and B exciton binding energies, found to be in agreement with the bulk exciton binding energy. We reveal the properties and evolution of the two species. We show that the excitons are trapped at very fast times (within a few picoseconds) and are present even at the highest pump fluences used (~8 μJ/cm^2), while the carriers are long-lived (≫1 ns).

EXPERIMENTAL METHODS

MoS_2 flakes were exfoliated from commercially available TMD powder by a liquid exfoliation method. A 10 mg/mL MoS_2 dispersion in *N*-methylpyrrolidone was sonicated by Qsonica Q700 probe sonicator with 50% power for 6 h. A 0 °C cooling bath and 10 s/2 s duty cycle were applied to avoid overheating. After sonication, the dispersion was centrifuged at 1500 rpm, and then at 7500 rpm, to remove unexfoliated particles and soluble impurities, respectively. The lateral dimension of the MoS_2 flakes ranged from 100 to 1000 nm similar to previous work.[11] The monoflake thin films were fabricated by a modified space-confined self-assembly method described in another paper.[8] In this work, hexane and water:acetonitrile (85:15, v/v) were used as top and bottom solvents, respectively. The MoS_2 dispersion was injected to the interface and formed a homogeneous thin film by self-assembly. After thin film deposition on glass substrates, the MoS_2 films were dried at RT and then annealed at 250 °C for 30 min in an inert atmosphere to remove all adsorbed solvent.

Ultrafast spectroscopy measurements were performed using the output pulses from a regenerative Ti:sapphire amplifier system (Astrella, Coherent) with time duration of ~30 fs, 800 nm center wavelength, repetition rate of 1 kHz, and energy of ~6 mJ/pulse. A fraction of the fundamental beam was frequency-converted in an optical parametric amplifier (OPA, Opera Solo, Coherent). For the TA spectroscopy measurements carried out in this study, output pulses at 600 and 410 nm served as excitation pulses. Another fraction of the beam was focused on a sapphire plate to generate broadband white light continuum pulses that were used as probe pulses and covered the spectral region between 450 and 750 nm. Probe pulses were sent through a delay stage and then noncollinearly focused on the sample where they overlapped spatially and temporally with the excitation pulses. The transmitted probe beam through the sample and the reference probe pulses were spectrally dispersed in home-built prism spectrometers (Entwicklungsbüro Stresing, Berlin) and detected separately by a pair of charge-coupled devices (CCD detectors, Hamamatsu S07030-0906). The spectrum of the differential transmission change of the probe pulses after photoexcitation was recorded for different time delays up to nanoseconds, while the pump pulses were chopped at 500 Hz for the signal to be measured shot by shot. The beam sizes of the excitation and probe pulses were ~1 mm and 250 μm, respectively, to ensure uniform distribution of detected photoexcited species.

RESULTS AND DISCUSSION

This work aims to present a series of results to evidence that photoexcitation of solution-processed MoS_2 nanoflakes results in the generation of a mixture of excitons and long-lived free charges at the direct band edge states, which show different signatures in the TA spectrum. Also, it gives a clear picture about the energy band diagram of these few-layer nanoflakes.

Figure 1a shows the TA spectra of the MoS_2 nanoflakes following photoexcitation at 600 nm, which corresponds to excitation above the B excitonic resonance, at an absorbed pump fluence of ~1.1 μJ/cm^2. Further analysis of the TA data to obtain the different temporal components necessary to describe the excited-state dynamics, shown in Figure 1b, are discussed later on. The maximum of the TA signal is reached within the time resolution of our experimental system (<80 fs). The TA spectra show highly structured features with a series of narrow positive and negative bands, comparable to previous reports for few-layer flakes.[12,25,26,30,31] The negative bands with peaks at 611 and 674 nm are observed at early times and are assigned to photobleaching (PB) of the excitonic B and A transitions, respectively.[12,25,26,30] The positive bands recorded on the low- and high-frequency sides of the excitonic PB peaks at early time delays have been attributed to carrier-induced peak broadening and/or pump-induced exciton line width broadening.[12,25,31] As seen in the inset of Figure 1a, the TA time profiles probed in resonance with the excitonic transitions

A and B evolve quickly (<20 ps), and then the dynamics remain almost constant for times up to 1 ns. Unexpectedly, the TA signal changes sign within 10 ps, and the TA spectra at later times are close to the mirror image of the early spectra. The new PB bands at later times are located at shorter wavelengths (~646 and ~589 nm) compared to the PB from the excitonic resonances.

We assign the blue-shifted PB peaks seen at late time delays in the few-layer MoS_2 nanoflakes to the presence of long-lived free charges in direct conduction/valence band states. The positive bands observed at the lower energy side of each PB peak are attributed to photoinduced absorption caused by the free charges. Thus, the energy difference between the PB bands at early and long times should reflect the exciton binding energy. To verify this suggestion, we take into consideration the band structure of MoS_2 at the K-point of the Brillouin zone, where the direct transitions take place. A simplified representation of the band diagram is shown in Figure 2. We

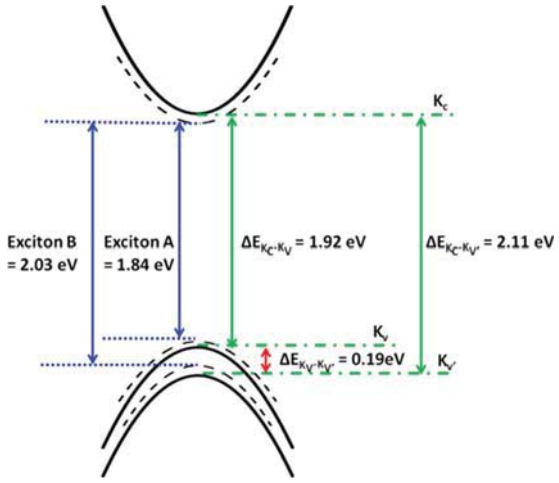

Figure 2. Simplified representation of the band diagram of the direct energy band gap (solid lines) and excitonic (dashed) states in MoS_2 nanoflakes at the K-point of the Brillouin zone.

note that the relatively large thickness of the nanoflakes used suggests that their energy band diagram is similar to that of the bulk material.[19] In Figure 2, the A and B excitonic states are denoted by dashed lines and lie below/above the conduction/valence band states. The absorption bands from the steady state spectrum define the A and B excitonic transition energies to be 2.03 eV (= 611 nm) and 1.84 eV (= 674 nm) (see Supporting Information, Figure S1), in agreement with the PB peaks in the TA data at early times. The two excitonic transitions are related to the same conduction band; thus, we make the simplified assumption that the energy difference between the two valence bands is equal to the energy difference between the A and B excitonic transitions ($\Delta E_{K_V-K_{V'}} \sim 0.19$ eV). Then, we use the blue-shifted PB band at 646 nm at long time delays (associated with free charges) to define that the energy difference between the conduction and valence band (K_C–K_V transition) is equal to $\Delta E_{K_C-K_V} \sim 1.92$ eV (= 646 nm). By taking the difference between the K_C–K_V band gap and the A excitonic transition energy, we find the exciton A binding energy to be ~80 meV, similar to the binding energy in the bulk material reported from theoretical and experimental studies.[33,34] By adding the energy difference between the two valence bands to the band gap, we find an energy difference between the K conduction band and the K' valence band equal to $\Delta E_{K_C-K_{V'}} \sim 2.11$ eV (= 587 nm), in agreement with the second PB band observed at long times. Finally, we extract the B exciton binding energy to be equal to ~83 meV.

This simple analysis supports that the unexpected behavior at longer times is associated with the observation of free charges at the direct conduction/valence bands. We thus evidence that photoexcitation above the direct excitonic transitions in thick MoS_2 nanoflakes (~10–20 atomic layers) results in the generation of a mixture of excitons and free charge carriers that show different signatures in the TA spectrum. The presence of free charges in few-layer MoS_2 nanoflakes has been suggested in previous studies.[30,31] However, the PB signatures of free charges at shorter wavelengths than the excitonic PB peaks, leading to an apparent change in the TA signal sign at long times, are reported here for the first time. We believe that the solution-based synthetic method used in our case—as discussed further below—and the large number of atomic layers (>10 layers) facilitate the formation of free charges, making their contribution evident in the TA spectra. The method followed for the processing of the nanoflakes can affect the trapping processes and thus the number of long-lived charges. Also, the increased thickness of the flakes makes them less sensitive to trapping via surface recombination.[29] Our nanosecond recombination lifetime for MoS_2 nanoflakes with >10 atomic layers is in agreement with a previous study.[29] More evidence that the blue-shifted PBs are the signatures of free charges will be extensively discussed below, based on pump fluence dependent measurements, TA results obtained following photoexcitation at 400 nm, and the similarities of our results to the results of Bordza et al., who also used MoS_2 nanoflakes synthesized via solvent exfoliation.[30]

A different possible interpretation of our experimental results could be that the observed change of the sign in the TA signals at long time delays is due to an increase of the absorption probability of the excitonic peaks. This effect would be observed when the photogenerated carriers cause a screening of the internal electric field potentially existing in the ground state material due to crystal piezoelectricity and has been previously reported in GaN thin films.[35] Piezoelectricity has been seen in a monolayer of MoS_2 due to lack of inversion symmetry; however, this mechanism is not expected to be present in 10–20 layer nanoflakes, as the symmetry is restored.[36]

To deconvolute the spectral components present in the TA spectra, we have analyzed the entire spectral and temporal pump–probe data sets using multiexponential global analysis. This involves analyzing the time profiles at all probe wavelengths using the same three time constants but allowing the pre-exponential amplitudes to vary freely. In this way, we can distinguish the amplitudes and time constants of different relaxation and recombination processes that influence the overall TA signal at different timescales. Furthermore, we can distinguish between the TA components related to the excitons and free charges and thus gain information about the species involved in each relaxation/recombination process.

Figure 1b shows the pre-exponential amplitude spectra associated with the three temporal components necessary to describe the excited-state dynamics. Similar multiexponential behavior has been previously reported in few-layer MoS_2.[12] Following an ultrafast initial rise of the TA features within the

experimental time resolution for all probe wavelengths, a fast relaxation component of hundreds of femtoseconds ($t_1 \sim 0.5$ ps), an intermediate one of a few picoseconds ($t_2 \sim 5.5$ ps), and a slow component ($\gg$1 ns) are resolved. Our analysis at this low pump fluence shows that the fast and intermediate relaxation components exhibit negative peaks at the excitonic resonances. Thus, we conclude that the fast and intermediate relaxation components are dominated by processes involving the excitons. Based on previous studies, the two components are related to exciton cooling and to fast trapping by trap states formed below the direct band gap.[12,28,37] For example, Nie et al. have performed TA experiments in few-layer MoS_2 nanoflakes using very short pulses (~10 fs) to show that carrier thermalization takes place within 20 fs via carrier−carrier and carrier−phonon scattering processes and carrier cooling occurs within ~0.6 ps.[25] Similar results have been reported via state-selective coherent multidimensional spectroscopy.[26] Exciton relaxation in trap/defect states was reported to occur on the few picosecond timescale, again in agreement with our results.[12] We cannot exclude that the time constant of ~0.5 ps is partly related to exciton splitting into charges as previously suggested; however, our pump fluence dependent measurements—discussed below—provide clear evidence that most of the charges are already present even at earlier time delays (they are generated faster than the experimental time resolution).[30] It is possible that there is a contribution of those instantaneously generated charges to the relaxation on the subpicosecond timescale, as suggested in a previous study.[31] However, we cannot gain further information about this relaxation of free charges at low pump fluence, since their spectrum coincidentally resembles the mirror image of the exciton spectrum and is therefore completely masked. The behavior of free charges at ultrafast timescales becomes more evident at higher pump fluences (see below). Once the excitons have become trapped within a few picoseconds, the remaining signatures in the TA spectra are related only to the free charges. Therefore, we additionally find the long-lived amplitude spectrum, where the PBs are located at higher photon energies compared to the excitonic PBs, representing the signature of free charges, which was previously not observed. The free charges live longer than the time window of our measurements (>1 ns).

To understand the influence of photoexcitation density on the exciton and free charge dynamics, pump fluence dependent transient measurements for excitation at 600 nm were performed. Absorbed pump fluences between 1.1 and 8.8 $\mu J/cm^2$ were used. The TA spectra at different time delays for the highest pump fluence (~8.8 $\mu J/cm^2$) are included in Figure 3a. For early delays, the TA spectra show quite similar behavior as the ones at the lowest pump fluence shown in Figure 1, but as the time evolves, the spectral features change at higher pump fluences. With higher excitation density, there is a gradual blue-shift of the TA spectra during the first 20 ps, and the signal at long time delays no longer mirrors the one at early time delays. This is also clear when the TA spectra at 0.1 ps and 1 ns are compared for different pump fluences in Figures 3b and 3c, respectively. At the early time delay, the TA amplitude scales linearly with the intensity, and the spectral shape is similar for all the pump fluences, without any evident spectral shift. This is because the amplitude of the TA signal at early times is mainly dominated by exciton signatures and not because charges are not present, as it is shown by the global analysis results shown and discussed below. On the other hand, at long times and at higher excitation densities, the long-lived TA component is

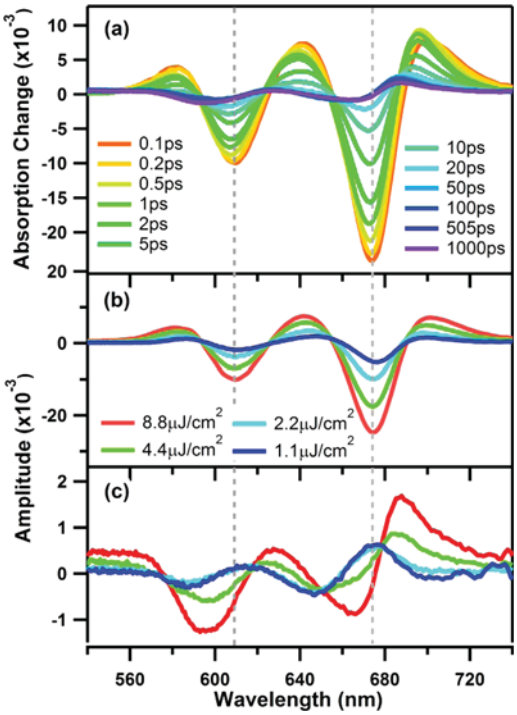

Figure 3. (a−c) TA spectra in few-layer MoS_2 nanoflakes following excitation at 600 nm at (a) different time delays and a pump fluence of ~8.8 $\mu J/cm^2$ and at different pump fluences between 1.1 and 8.8 $\mu J/cm^2$ at (b) early (t = 0.1 ps) and (c) long times (t = 1 ns).

increasingly red-shifted. As discussed below, this is due to bandgap renormalization (BGR) effects. Similar observations were obtained by additional TA measurements performed with excitation at higher photon energy of 3 eV (= 410 nm) (Figure S2a−c, included in the Supporting Information). The most pronounced difference between excitation at 600 and 410 nm is seen in the TA spectra at long time delays, where a higher density of free charges is long-lived. This is expected since the excess kinetic energy that the carriers obtain during photoexcitation with photon energies well above the direct band gap facilitates the formation of free charges. This is additional evidence that the blue-shifted PBs seen at long timescales are the signature of free charges.

The gradual blue-shift of the TA spectra with time that we see here (most pronounced at high pump fluences, Figure 3a), has been previously observed, but not the gradual evolution into a mirror image spectral shape, which we observe at low fluence (Figure 1a). Previously, the blue-shifted TA spectra have been assigned to the presence of free charges by Bordza et al., while Cunnigham et al. have related it to line width broadening and a red-shift in absorption at early times caused by BGR due to excitons.[30,31] We believe that the different assignments originate from the different free charge densities obtained following photoexcitation of nanoflakes synthesized by different methods. Our results at high pump fluences show similar behavior as the ones of Borzda et al., where they proposed that the blue-shifted TA spectrum is due to the presence of free charges. In this study, MoS_2 nanoflakes synthesized via solvent exfoliation were also used. Thus, in solution-processed MoS_2 nanoflakes, the different dynamics governing the decay of excitons and charges, as shown by our global analysis, are responsible for the observed blue-shift at early times. The PB due to the excitonic transitions probed at

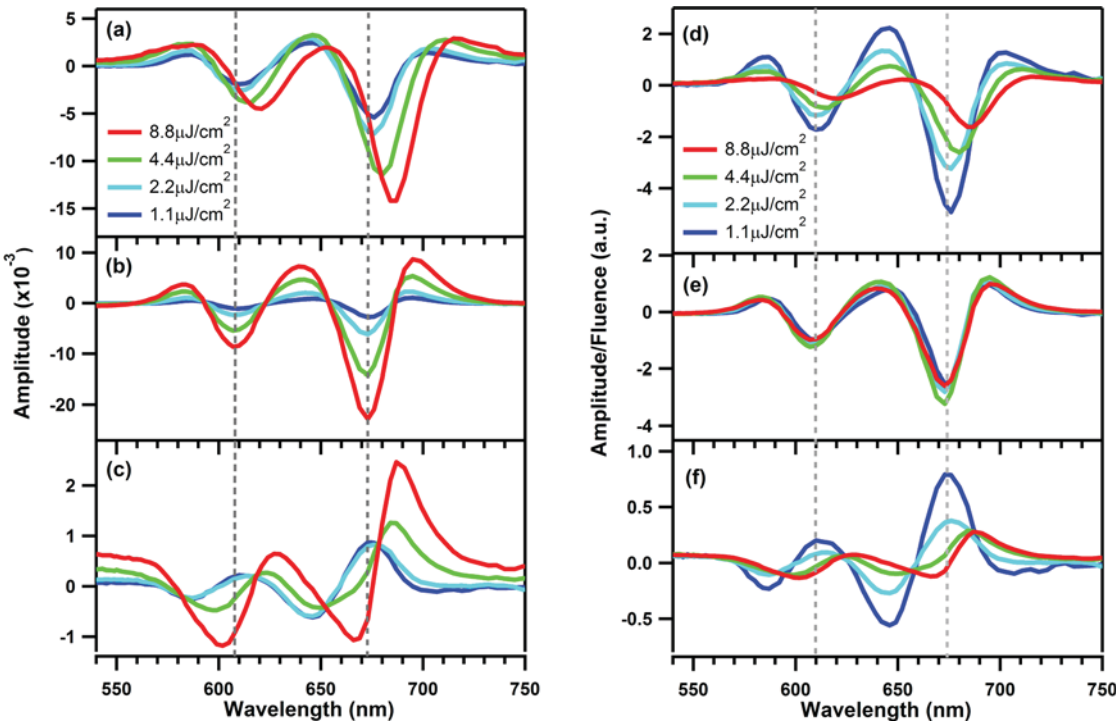

Figure 4. (a–c) Amplitude spectra from multiexponential global analysis of the TA data, at different pump fluences between 1.1 and 8.8 $\mu J/cm^2$ for the fast time constant of 0.5 ps (a), the intermediate one of 5.5 ps (b), and the long component (c). (d, e) The respective amplitude spectra scaled with the pump fluence for the fast (d), the intermediate one (e), and the long component (f).

longer wavelengths decay much faster than the PB peaks due to the long-lived charges, shifting the overall TA spectrum to shorter wavelengths toward the signatures of the charges within 10 ps. This leads to an evident blue-shift with time at higher fluences (where the energy bands are affected by BGR). At low pump fluence, the PB bands of the charges are even more blue-shifted but coincide with the positive spectral features of the excitons and vice versa, which leads to an apparent evolution into a mirror image spectral shape. This behavior is a coincidence caused by the particular exciton binding energy of our sample.

On the other hand, Cunningham et al. studied MoS_2 monolayers and multilayers synthesized via chemical vapor deposition (CVD). In this case, we note that the blue-shift seen for similar pump fluences is smaller (few meV) compared to the one reported in our case and by Bordza et al., which is tens of meV. This is expected, since the red-shift caused by BGR of excitons is competing with a blue-shift due to the screening between opposite charges, resulting in a weak overall spectral shift that is maximum for times close to zero where also the exciton density is maximum. As the time delay increases the excitons recombine and the contribution from BGR is reduced; thus, the energy states are shifted to higher photon energies causing the PB to blue-shift with time. To compare our data with the work by Cunningham et al., we plotted the TA spectra at the lowest pump fluence used—where no blue-shift due to the presence of charges is observed—for time delays up to 3 ps in Figure S3 (Supporting Information). A small blue-shift is observed with time, in agreement with Cunningham et al.[31] However, further investigation of the induced line width broadening is out of the scope of this work, since it has been studied previously.[27,31]

Further insight into the relaxation/recombination dynamics of both excitons and charges has been obtained by multi-exponential global analysis of the TA spectra for all the fluences used. The amplitude spectra for the fast, intermediate, and slow time constants for excitation at 600 nm are shown in Figure 4a–c. No significant change is seen in the three time constants used to describe the temporal evolution of the TA signal at different pump fluences. However, as the excitation density increases, the amplitude spectra of the fast and slow time constants are increasingly red-shifted, but this is not the case for the intermediate component. This is also valid for the amplitude spectra of the three temporal components scaled by the pump fluence shown in Figure 4d,e. These confirm a linear dependence of the overall signal amplitude with pump fluence for the intermediate component attributed to exciton trapping, in contrast to the sublinear and red-shifting behavior of the fast and slow components.

The spectral red-shift at high carrier densities of the long-lived component (Figures 4c and 4f) is a clear sign that many-body interactions between the free charges are responsible for these changes. The repulsive Coulomb interactions between the photoexcited charges, which fill the edges of the conduction/valence band states, cause a band gap shrinkage, an effect known as band gap renormalization (BGR). This is expected to induce a red-shift of the PB bands at higher pump fluences, in agreement with our experimental observations.[38] In multilayer MoS_2 synthesized via solvent exfoliation, large red-shifts were previously observed for the long-lived component, attributed to the presence of BGR due to charges.[30] In addition, recent theoretical and experimental studies underline the strong contribution of BGR effects caused by the presence of charges in 2D metal dichalcogenides with high exciton binding energy.[38,39] For example, in our case, for the maximum absorbed pump fluence used (~8.8 $\mu J/cm^2$), a red-shift of the PB peaks of ~54 meV is measured at a time delay of 1 ns compared to the lowest used fluence of ~1.1 $\mu J/cm^2$.

As in the case of quantum wells, the wavelength of the PB at the excitonic transitions should not be significantly affected by the photoexcited carrier density, since the red-shift due to BGR is compensated by a blue-shift due to screening of the attractive interaction between opposite charges, reducing the exciton binding energy. This is consistent with the intermediate component of t_2 = 5.5 ps, where the excitonic peak positions are unaffected by pump fluence (Figures 4b and 4e). This component can thus clearly be attributed to the trapping of excitons, which is independent of excitation density in the investigated range. Also, the linear dependence of the intermediate spectral amplitude on the pump fluence shows the absence of higher order recombination effects for the photogenerated excitons.

The spectral behavior of the fast component (Figures 4a and 4d) brings more insight into the relaxation of both excitons and charges at early time delays following photoexcitation. At low pump fluences, the amplitude spectrum of the fast (0.5 ps) component is similar to the one of the intermediate component, showing that exciton relaxation dominates the early dynamics, as discussed before. Since the signature of the charges is coincidentally the mirror image of the exciton signature, any relaxation of charges at early times is masked, as it does not alter the spectral shape other than reducing the overall TA amplitude. However, the sublinear fluence dependence of the fast component at high excitation densities resembles the one of the slow component due to free charges, suggesting a contribution of charge dynamics (e.g., relaxation to trap states) even at very early time delays. The sublinear behavior of the fast component cannot derive from higher order exciton recombination processes like exciton−exciton annihilation, since this would also result in a sublinear fluence dependence of the early TA spectrum at 0.1 ps (Figure 3b) and of the amplitude spectrum related to the intermediate time constant (exciton trapping, Figures 4b and 4e), which is linear with excitation density. Also, if the fast component was due to exciton−exciton annihilation, a larger contribution at higher pump fluences would be expected, which is not the case. The fact that the fast component is affected by charge carrier relaxation is further supported by the spectral red-shift seen at the higher pump fluences. This is a clear indication that the contribution from free charges becomes more prominent and leads to BGR effects even at short timescales. Thus, shifted PBs due to free charges are evident at fast timescales and high fluence. The fast relaxation component seems to involve more charges at higher pump fluences, which is probably related to the presence of nonlinear effects like Auger recombination. This fast recombination of charges at higher fluence causes the sublinear increment of the long-lived charge component, shown in the Figure 4f. Our conclusions are further confirmed by the global analysis of the TA data with 410 nm excitation included in the Supporting Information (Figure S4).

In the work by Bordza et al., the generation of free charges was related to the dissociation of excitons with a time constant of 700 fs. This conclusion was based on the different rise time between the PBs and positive TA signatures at early times. In our case, the rise times for all peaks are pulse-width limited (<100 fs). The kinetic analysis followed by Bordza et al. was performed for data recorded at high pump fluences, where BGR effects are expected. Thus, we cannot exclude that the differences compared to our work are due to the higher photoexcited carried densities.[30] Overall, our results strongly support that free charges are already present at ultrafast timescales, generated during photoexcitation, and not formed via slower exciton dissociation.

CONCLUSIONS

In summary, we have examined the photophysical properties of solution-processed few-layer MoS_2 nanoflakes via ultrafast transient absorption spectroscopy. Throughout the paper, we provide evidence that the photoexcitation above the direct band gap in multilayer MoS_2 nanoflakes results in a mixture of both charges and excitons at ultrafast times. While the existence of both free charges and excitons has been reported by other groups,[30,31] we provide clear evidence that we probe free charges at the direct band edge states, which was not shown before. This is also the first time that free charges are observed to have a significantly distinguished signature from excitons, as expected from the large exciton binding energy of this material. The energy levels of the conduction and valence bands found in our study are supported by the extracted exciton binding energy that is in agreement with the one of the bulk material (~80 meV). We show that the excitons are trapped on the picosecond timescale and are present even at the highest absorbed pump fluence used (~8 $\mu J/cm^2$), while the carriers are long-lived ($\gg$1 ns). Our results are in agreement with previous work on MoS_2 nanoflakes synthesized also via solvent exfoliation but differ from studies on nanoflakes obtained by different processing routes.[30] Many-body interactions between free charges are evident at high photoexcited carrier densities, resulting in bandgap renormalization effects. The presence of those effects even at <1 ps timescales evidence that the generation of free charges occurs during photoexcitation and is not related to subsequent exciton splitting. We believe that solvent exfoliation used for the nanoflake synthesis results in higher densities of free charges. Moreover, we cannot exclude that the thicker nanoflakes used here also facilitate the generation of free charges with long lifetimes, as suggested previously.[29] The optoelectronic properties of the nanoflakes revealed by this study, such as the generation of long-lived charge carriers, suggest that the solution-based processing techniques used to prepare the MoS_2 thin films are suitable for applications in energy conversion.

ASSOCIATED CONTENT

Supporting Information

The Supporting Information is available free of charge on the ACS Publications website at DOI: 10.1021/acs.jpcc.6b09267.

Information about the steady-state absorbance spectrum of solution-processed MoS_2 nanoflakes; additional TA data and analysis (PDF)

AUTHOR INFORMATION

Corresponding Authors

*(D.T.) E-mail dimitra.tsokkou@unifr.ch; phone +41 (0)26 300 8696.

*(N.B.) E-mail natalie.banerji@unifr.ch; phone +41 (0)26 300 8698.

Notes

The authors declare no competing financial interest.

ACKNOWLEDGMENTS

D.T. and N.B. thank the Swiss National Science Foundation (grant PP00P2_150536, NCCR-MUST) and the University of Fribourg for funding.

REFERENCES

(1) Chhowalla, M.; Shin, H. S.; Eda, G.; Li, L.-J.; Loh, K. P.; Zhang, H. The Chemistry of Two-Dimensional Layered Transition Metal Dichalcogenide Nanosheets. *Nat. Chem.* **2013**, *5*, 263−275.

(2) Tan, C.; Zhang, H. Two-Dimensional Transition Metal Dichalcogenide Nanosheet-Based Composites. *Chem. Soc. Rev.* **2015**, *44*, 2713−2731.

(3) Niu, L.; Coleman, J. N.; Zhang, H.; Shin, H.; Chhowalla, M.; Zheng, Z. Production of Two-Dimensional Nanomaterials via Liquid-Based Direct Exfoliation. *Small* **2016**, *12*, 272−293.

(4) Evans, B. L.; Young, P. A. Exciton Spectra in Thin Crystals: the Diamagnetic Effect. *Proc. Phys. Soc., London* **1967**, *91*, 475.

(5) Mak, K. F.; Lee, C.; Hone, J.; Shan, J.; Heinz, T. F. Atomically Thin MoS_2: A New Direct-Gap Semiconductor. *Phys. Rev. Lett.* **2010**, *105*, 136805.

(6) Kuc, A.; Zibouche, N.; Heine, T. Influence of Quantum Confinement on the Electronic Structure of the Transition Metal Sulfide TS_2. *Phys. Rev. B: Condens. Matter Mater. Phys.* **2011**, *83*, 245213.

(7) Wang, Q. H.; Kalantar-Zadeh, K.; Kis, A.; Coleman, J. N.; Strano, M. S. Electronics and Optoelectronics of Two-Dimensional Transition Metal Dichalcogenides. *Nat. Nanotechnol.* **2012**, *7*, 699−712.

(8) Yu, X.; Prevot, M. S.; Guijarro, N.; Sivula, K. Self-Assembled 2D WSe_2 Thin Films for Photoelectrochemical Hydrogen Production. *Nat. Commun.* **2015**, *6*, 7596.

(9) Li, H.; Wu, J.; Yin, Z.; Zhang, H. Preparation and Applications of Mechanically Exfoliated Single-Layer and Multilayer MoS_2 and WSe_2 Nanosheets. *Acc. Chem. Res.* **2014**, *47* (4), 1067−1075.

(10) Zhang, W.; Zhang, P.; Su, Z.; Wei, G. Synthesis and Sensor Applications of MoS_2-Based Nanocomposites. *Nanoscale* **2015**, *7*, 18364−18378.

(11) Yu, X.; Prévot, M. S.; Sivula, K. Multiflake Thin Film Electronic Devices of Solution Processed 2D MoS_2 Enabled by Sonopolymer Assisted Exfoliation and Surface Modification. *Chem. Mater.* **2014**, *26*, 5892−5899.

(12) Shi, H.; Yan, R.; Bertolazzi, S.; Brivio, J.; Gao, B.; Kis, A.; Jena, D.; Xing, H. G.; Huang, L. Exciton Dynamics in Suspended Monolayer and Few-Layer MoS_2 2D Crystals. *ACS Nano* **2013**, *7*, 1072−1080.

(13) Wang, Q.; Ge, S.; Li, X.; Qiu, J.; Ji, Y.; Feng, J.; Sun, D. Valley Carrier Dynamics in Monolayer Molybdenum Disulfide from Helicity-Resolved Ultrafast Pump−Probe Spectroscopy. *ACS Nano* **2013**, *7*, 11087−11093.

(14) Lagarde, D.; Bouet, L.; Marie, X.; Zhu, C. R.; Liu, B. L.; Amand, T.; Tan, P. H.; Urbaszek, B. Carrier and Polarization Dynamics in Monolayer MoS_2. *Phys. Rev. Lett.* **2014**, *112*, 047401.

(15) Mai, C.; Barrette, A.; Yu, Y.; Semenov, Y. G.; Kim, K. W.; Cao, L.; Gundogdu, K. Many-Body Effects in Valleytronics: Direct Measurement of Valley Lifetimes in Single-Layer MoS_2. *Nano Lett.* **2014**, *14*, 202−206.

(16) Sun, D.; Rao, Y.; Reider, G. A.; Chen, G.; You, Y.; Brézin, L.; Harutyunyan, A. R.; Heinz, T. F. Observation of Rapid Exciton−Exciton Annihilation in Monolayer Molybdenum Disulfide. *Nano Lett.* **2014**, *14*, 5625−5629.

(17) Docherty, C. J.; Parkinson, P.; Joyce, H. J.; Chiu, M.-H.; Chen, C.-H.; Lee, M.-Y.; Li, L.-J.; Herz, L. M.; Johnston, M. B. Ultrafast Transient Terahertz Conductivity of Monolayer MoS_2 and WSe_2 Grown by Chemical Vapor Deposition. *ACS Nano* **2014**, *8*, 11147−11153.

(18) Pogna, E. A. A.; Marsili, M.; De Fazio, D.; Dal Conte, S.; Manzoni, C.; Sangalli, D.; Yoon, D.; Lombardo, A.; Ferrari, A. C.; Marini, A.; Cerullo, G.; Prezzi, D. Photo-Induced Bandgap Renormalization Governs the Ultrafast Response of Single-Layer MoS_2. *ACS Nano* **2016**, *10*, 1182−1188.

(19) Splendiani, A.; Sun, L.; Zhang, Y.; Li, T.; Kim, J.; Chim, C.-Y.; Galli, G.; Wang, F. Emerging Photoluminescence in Monolayer MoS_2. *Nano Lett.* **2010**, *10*, 1271−1275.

(20) Lui, C. H.; Frenzel, A. J.; Pilon, D. V.; Lee, Y. H.; Ling, X.; Akselrod, G. M.; Kong, J.; Gedik, N. Trion-Induced Negative Photoconductivity in Monolayer MoS_2. *Phys. Rev. Lett.* **2014**, *113*, 166801.

(21) Mak, K. F.; He, K.; Lee, C.; Lee, G. H.; Hone, J.; Heinz, T. F.; Shan, J. Tightly Bound Trions in Monolayer MoS_2. *Nat. Mater.* **2013**, *12*, 207−211.

(22) Sie, E. J.; Frenzel, A. J.; Lee, Y.-H.; Kong, J.; Gedik, N. Intervalley Biexcitons and Many-Body Effects in Monolayer MoS_2. *Phys. Rev. B: Condens. Matter Mater. Phys.* **2015**, *92*, 125417.

(23) Radisavljevic, B.; Radenovic, A.; Brivio, J.; Giacometti, V.; Kis, A. Single-Layer MoS_2 Transistors. *Nat. Nanotechnol.* **2011**, *6*, 147−150.

(24) Das, S.; Chen, H.-Y.; Penumatcha, A. V.; Appenzeller, J. High Performance Multilayer MoS_2 Transistors with Scandium Contacts. *Nano Lett.* **2013**, *13*, 100−105.

(25) Nie, Z.; Long, R.; Sun, L.; Huang, C.-C.; Zhang, J.; Xiong, Q.; Hewak, D. W.; Shen, Z.; Prezhdo, O. V.; Loh, Z.-H. Ultrafast Carrier Thermalization and Cooling Dynamics in Few-Layer MoS_2. *ACS Nano* **2014**, *8*, 10931−10940.

(26) Czech, K. J.; Thompson, B. J.; Kain, S.; Ding, Q.; Shearer, M. J.; Hamers, R. J.; Jin, S.; Wright, J. C. Measurement of Ultrafast Excitonic Dynamics of Few-Layer MoS_2 Using State-Selective Coherent Multidimensional Spectroscopy. *ACS Nano* **2015**, *9*, 12146−12157.

(27) Sim, S.; Park, J.; Song, J.-G.; In, C.; Lee, Y.-S.; Kim, H.; Choi, H. Exciton Dynamics in Atomically Thin MoS_2: Interexcitonic Interaction and Broadening Kinetics. *Phys. Rev. B: Condens. Matter Mater. Phys.* **2013**, *88*, 075434.

(28) Kar, S.; Su, Y.; Nair, R. R.; Sood, A. K. Probing Photoexcited Carriers in a Few-Layer MoS_2 Laminate by Time-Resolved Optical Pump−Terahertz Probe Spectroscopy. *ACS Nano* **2015**, *9*, 12004−12010.

(29) Wang, H.; Zhang, C.; Rana, F. Surface Recombination Limited Lifetimes of Photoexcited Carriers in Few-Layer Transition Metal Dichalcogenide MoS_2. *Nano Lett.* **2015**, *15*, 8204−8210.

(30) Borzda, T.; Gadermaier, C.; Vujicic, N.; Topolovsek, P.; Borovsak, M.; Mertelj, T.; Viola, D.; Manzoni, C.; Pogna, E. A. A.; Brida, D.; Antognazza, M. R.; Scotognella, F.; Lanzani, G.; Cerullo, G.; Mihailovic, D. Charge Photogeneration in Few-Layer MoS_2. *Adv. Funct. Mater.* **2015**, *25*, 3351−3358.

(31) Cunningham, P. D.; McCreary, K. M.; Hanbicki, A. T.; Currie, M.; Jonker, B. T.; Hayden, L. M. Charge Trapping and Exciton Dynamics in Large-Area CVD Grown MoS_2. *J. Phys. Chem. C* **2016**, *120*, 5819−5826.

(32) Strait, J. H.; Nene, P.; Rana, F. High Intrinsic Mobility and Ultrafast Carrier Dynamics in Multilayer Metal-Dichalcogenide MoS_2. *Phys. Rev. B: Condens. Matter Mater. Phys.* **2014**, *90*, 245402.

(33) Komsa, H.-P.; Krasheninnikov, A. V. Effects of Confinement and Environment on the Electronic Structure and Exciton Binding Energy of MoS_2 from First Principles. *Phys. Rev. B: Condens. Matter Mater. Phys.* **2012**, *86*, 241201.

(34) Ramasubramaniam, A. Large Excitonic Effects in Monolayers of Molybdenum and Tungsten Dichalcogenides. *Phys. Rev. B: Condens. Matter Mater. Phys.* **2012**, *86*, 115409.

(35) Omae, K.; Kawakami, Y.; Fujita, S.; Yamada, M.; Narukawa, Y.; Mukai, T. Effects of Internal Electric Field and Carrier Density on Transient Absorption Spectra in a Thin GaN Epilayer. *Phys. Rev. B: Condens. Matter Mater. Phys.* **2002**, *65*, 073308.

(36) Wu, W.; Wang, L.; Li, Y.; Zhang, F.; Lin, L.; Niu, S.; Chenet, D.; Zhang, X.; Hao, Y.; Heinz, T. F.; Hone, J.; Wang, Z. L. Piezoelectricity of Single-Atomic-Layer MoS_2 for Energy Conversion and Piezotronics. *Nature* **2014**, *514*, 470−474.

(37) Wang, H.; Zhang, C.; Rana, F. Ultrafast Dynamics of Defect-Assisted Electron−Hole Recombination in Monolayer MoS_2. *Nano Lett.* **2015**, *15*, 339−345.

(38) Chernikov, A.; Ruppert, C.; Hill, H. M.; Rigosi, A. F.; Heinz, T. F. Population Inversion and Giant Bandgap Renormalization in Atomically Thin WS_2 Layers. *Nat. Photonics* **2015**, *9*, 466−470.

(39) Steinhoff, A.; Rösner, M.; Jahnke, F.; Wehling, T. O.; Gies, C. Influence of Excited Carriers on the Optical and Electronic Properties of MoS_2. *Nano Lett.* **2014**, *14*, 3743−3748.